Semiconductor Science and Technology

PAPER

Organic passivation of $Al_{0.5}Ga_{0.5}N$ epilayers using self-assembled monolayer of Zn(II) porphyrin for improved solar-blind photodetector performance

IOP Publishing Semiconductor Science and Technology
Semicond. Sci. Technol. **36** (2021) 055001 (9pp) https://doi.org/10.1088/1361-6641/abeb84

Organic passivation of $Al_{0.5}Ga_{0.5}N$ epilayers using self-assembled monolayer of Zn(II) porphyrin for improved solar-blind photodetector performance

Shuchi Kaushik[1], Tejas R Naik[2], M Ravikanth[3], Che-Hao Liao[4], Xiaohang Li[4], V Ramgopal Rao[2,5] and R Singh[1,6,*]

[1] Department of Physics, Indian Institute of Technology Delhi, Hauz Khas, New Delhi 110016, India
[2] Centre of Excellence in Nanoelectronics, Indian Institute of Technology Bombay, Mumbai, Maharashtra 400076, India
[3] Department of Chemistry, Indian Institute of Technology Bombay, Mumbai, Maharashtra 400076, India
[4] Advanced Semiconductor Laboratory, King Abdullah University of Science and Technology (KAUST), Thuwal 23955-6900, Saudi Arabia
[5] Department of Electrical Engineering, Indian Institute of Technology Delhi, Hauz Khas, New Delhi 110016, India
[6] Nanoscale Research Facility, Indian Institute of Technology Delhi, Hauz Khas, New Delhi 110016, India

E-mail: rsingh@physics.iitd.ac.in

Received 20 January 2021, revised 26 February 2021
Accepted for publication 3 March 2021
Published 29 March 2021

Abstract

We report on the passivation of surface states of $Al_{0.5}Ga_{0.5}N$ epilayers by employing self-assembled monolayers (SAMs) of organic molecules, which led to a significant improvement in the performance of $Al_{0.5}Ga_{0.5}N$ based solar-blind photodetector. The formation of SAM of meso-(5-hydroxyphenyl)-10,15,20-tri(p-tolyl) porphyrin (ZnTPP(OH)) on the surface of $Al_{0.5}Ga_{0.5}N$ was probed by contact angle measurement, x-ray photoelectron spectroscopy, and atomic force microscopy. The successful passivation of surface states was confirmed by Kelvin probe force microscopy as a significant decrease in the surface potential of $Al_{0.5}Ga_{0.5}N$ by ∼280 mV was observed. The inference was supported by a four-fold increase in the photoluminescence intensity of the near-band edge emission peak upon passivation. As a result, the dark current of the as-fabricated solar-blind photodetector reduced by two orders of magnitude, without compromising with the magnitude of the photo current at 270 nm. The role of SAM was evident in improving the performance of the photodetector as the peak value of photo-to-dark current ratio enhanced by ∼36 times. The peak responsivity of the photodetector increased from 1.6 to 2.2 mA W^{-1} at 10 V. The significant reduction in the dark current and enhancement in the responsivity led to an improvement in the specific detectivity by ∼10 times. Additionally, the response speed of the photodetector was found to improve significantly from 4 to 0.5 s.

* Author to whom any correspondence should be addressed.

Keywords: surface states, passivation, self-assembled monolayer, solar-blind photodetector, responsivity, dark current, temporal response

(Some figures may appear in colour only in the online journal)

1. Introduction

The efficient detection of ultraviolet (UV) light is vital for a wide range of applications such as disinfecting bio-agents, water purification, flame detection, early missile warning systems, UV dosimetry, UV astronomy, and space missions [1–3]. For most of these applications, along with UV detection, it is important to get rid of background signals of visible or infra-red radiations from the sun. This has led to the focus on fabricating state-of-the-art 'solar-blind' photodetectors. A solar-blind photodetector is the one which is insensitive to the photons with wavelengths longer than ∼285 nm [4–8]. The wide bandgap semiconductors, viz. $Al_xGa_{1-x}N$, AlN, SiC, Ga_2O_3 and diamond are suitable for fabricating such photodetectors [8–10]. Out of these semiconductors, $Al_xGa_{1-x}N$, the alloy of GaN and AlN, has a direct bandgap which can be tuned from 3.4 eV ($x = 0$) to 6.2 eV ($x = 1$). The alloys with higher concentrations of Al ($x \geqslant 0.5$) are suitable for realizing solar-blind operation [11]. Furthermore, the material exhibits extraordinary properties of high temperature robustness, chemical and radiation hardness, making it the preferable candidate for fabricating robust solar-blind photodetectors [8, 12–17]. However, $Al_xGa_{1-x}N$ is plagued with a large density of surface states ($\sim 10^{13}$ charges cm^{-2}). As a result of these surface states, trap-assisted tunneling (TAT) becomes one of the dominant current transport mechanisms which leads to a large dark current in the photodetectors [18–21]. The increase in dark current results in poor photo-to-dark current ratio (PDCR), responsivity, and speed of the photodetector, thereby degrading its performance [18, 22, 23]. Therefore, to realize the true potential of $Al_xGa_{1-x}N$ for solar-blind photodetection, it is necessary to passivate these surface states.

In this work, we have opted for a bottom-up approach based on self-assembled monolayers (SAMs) of porphyrin (ZnTPP(OH)) to passivate the surface states of $Al_{0.5}Ga_{0.5}N$ epilayer grown over AlN template on sapphire (refer to figures 1(a)–(c)). Consequently, the performance of metal–semiconductor–metal (MSM) solar-blind photodetector fabricated on passivated $Al_{0.5}Ga_{0.5}N$ epilayer (shown in figure 1(d)) was found to improve significantly. The ZnTPP(OH) molecule can be visualized to consist of three parts: a head group, an end group and a backbone. The head group is chemically bonded to the hydroxylated $Al_{0.5}Ga_{0.5}N$ epilayer, as illustrated in figure 1(e) (explained later). The end group remains away from the $Al_{0.5}Ga_{0.5}N$ surface, and backbone links the head group to the end group [24–28]. The reported method of wet passivation opens up the route to easily reproducible, less error-prone and cost-effective passivation schemes for $Al_xGa_{1-x}N$, which can improve the performance of $Al_xGa_{1-x}N$ based electronic and optoelectronic devices remarkably.

2. Experimental

The 0.5 μm thick $Al_{0.5}Ga_{0.5}N$ epitaxial film used in this work was grown over AlN template on sapphire using metal organic chemical vapor deposition (MOCVD, Taiyo Nippon Sanso, SR4000 HT) as represented in figure 1(a). The 2Theta-omega curve of the as-grown sample was measured using x-ray diffraction (XRD, Bruker, D8 Discover) and is shown in figure 1(b). The peaks corresponding to (0002) and (0004) planes of AlGaN and AlN were obtained. The presence of (0002) $Al_{0.5}Ga_{0.5}N$ peak at 35.241° (shown in figure 1(c)) corresponds to ∼50% Al content in the film. The wafer was diced into small samples of size 5 mm × 5 mm, which were cleaned in de-ionized (DI) water, acetone, and isopropyl alcohol (IPA) using the standard procedure [26]. For the passivation, the surface of bare $Al_{0.5}Ga_{0.5}N$ was activated by immersing in H_2SO_4:H_2O_2 (3:1) solution for 20 min [29]. The samples obtained thereafter were referred to as the hydroxylated samples. The hydroxylated samples were rinsed with DI water and dipped into ZnTPP(OH) solution (prepared by dissolving 1 mg ZnTPP(OH) compound in 5 ml Toluene) for an optimized time of 2 h [26]. After this, the samples were rinsed with IPA, dried using dry nitrogen, and were placed in hot air oven at 120 °C for 10 min. The samples prepared by the above process were named SAM passivated samples. Both bare and passivated films were characterized by contact angle measurement (CA, Data Physics), x-ray photoelectron spectroscopy (XPS, PHI 5000 Versa Probe II), atomic force microscopy (AFM, Asylum Research, MFP 3D), Kelvin probe force microscopy (KPFM, Bruker Dimension ICON) and photoluminescence spectroscopy (PL, Horiba, LabRAM HR Evolution). To study the effect of passivation on the device performance, the interdigitated geometry of MSM photodetectors (with 50 μm electrode width and inter-electrode spacing) was fabricated on both bare and SAM passivated $Al_{0.5}Ga_{0.5}N$ films using mask-less optical lithography (Intelligent Micropatterning SF-100 Xpress), and Ni/Au (30 nm/40 nm) metals were deposited using thermal evaporation (base pressure $\sim 10^{-6}$ Torr). Finally, lift-off was performed in warm acetone to obtain Ni/Bare $Al_{0.5}Ga_{0.5}N$/Ni and Ni/SAM $Al_{0.5}Ga_{0.5}N$/Ni MSM photodetectors. The photodetectors were tested in dark and under illumination by Keithley semiconductor characterization system (SCS-4200) connected to the EverBeing DC probe station (EB-6). For photodetection measurements, an assembly of Xenon lamp (75 W), monochromator (Bentham TMC 300), optical fiber

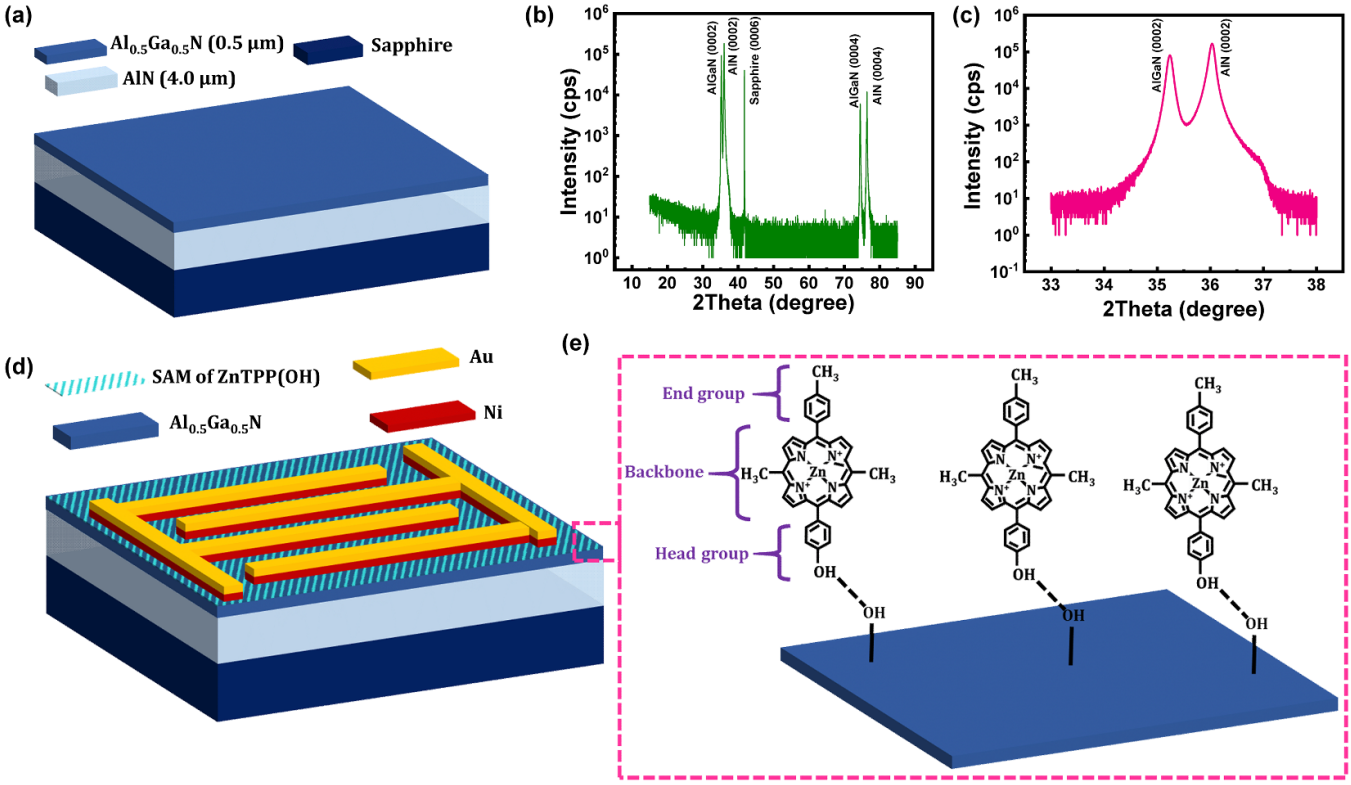

Figure 1. (a) The schematic representation of the sample showing 0.5 μm thick $Al_{0.5}Ga_{0.5}N$ grown over AlN template on sapphire. (b) The XRD 2Theta-omega curve of the as-grown sample. (c) The zoomed view of the 2Theta-omega curve showing peaks corresponding to (0002) plane of $Al_{0.5}Ga_{0.5}N$ and AlN. (d) The schematic representation of as-fabricated MSM photodetector on SAM passivated $Al_{0.5}Ga_{0.5}N$ epilayer. (e) The schematic showing the bonding of ZnTPP(OH) molecules with the –OH groups of hydroxylated $Al_{0.5}Ga_{0.5}N$ to form SAM.

(PCU-1000), power meter and sensor (Thor Laboratories) was used.

3. Results and discussion

3.1. Characterization of SAM

In order to confirm the presence of molecular layer onto the $Al_{0.5}Ga_{0.5}N$ surface, water CA measurement and XPS were performed. As shown in figure 1(e), the end group ($-CH_3$) of the ZnTPP(OH) molecule is a hydrophobic group [28]. Therefore, the first test to examine the presence of SAM was the CA measurement. The CAs of bare, hydroxylated and SAM passivated $Al_{0.5}Ga_{0.5}N$ films are shown in figure 2(a). For bare film, the observed value of CA was 78°. The process of hydroxylation led to the formation of hydroxyl groups (–OH) on the surface of $Al_{0.5}Ga_{0.5}N$, thereby reducing CA to 42°. A high CA of 98° was observed for SAM passivated film, which assured the presence of a hydrophobic layer on the $Al_{0.5}Ga_{0.5}N$ surface [28]. Moreover, CA of >90° indicated the presence of $-CH_3$ groups on the top surface which implied vertically standing molecules on the $Al_{0.5}Ga_{0.5}N$ surface (as shown in figure 1(e)). In order to investigate the bonding between the molecular layer and the $Al_{0.5}Ga_{0.5}N$ surface, we opted for the surface sensitive XPS characterization of the SAM passivated film. Figures 2(b)–(f) show Zn 2p peaks and the deconvoluted peaks for N 1s, Ga $2p_{3/2}$, Al 2p, and O 1s. The Zn $2p_{3/2}$ and Zn $2p_{1/2}$ peaks (figure 2(b)) at 1021.24 eV and 1044.34 eV [26, 30], respectively, indicate the presence of ZnTPP(OH) monolayer on the $Al_{0.5}Ga_{0.5}N$ surface. Along with Zn peaks, the peaks corresponding to N in TPP at 396.71 eV (figure 2(c)) [30–32], and HO–C at 532.32 eV (figure 2(f)) [26, 31] also highlight the presence of ZnTPP(OH) SAM. The peaks corresponding to Ga–OH at 1118.18 eV (figure 2(d)) [30], Al–OH at 74.01 eV (figure 2(e)) [26, 33], HO–Ga at 530.66 eV [30], and HO–Al at 529.93 eV (figure 2(f)) indicate the existence of –OH groups on $Al_{0.5}Ga_{0.5}N$ surface. Finally, the peak at 531.54 eV [34] in O 1s spectra (figure 2(f)) corresponds to HO–OH bond between the –OH groups of the hydroxylated $Al_{0.5}Ga_{0.5}N$ surface and the ZnTPP(OH) molecule. These results confirm the chemical adsorption of SAM on $Al_{0.5}Ga_{0.5}N$ surface.

3.2. Effect of SAM on $Al_{0.5}Ga_{0.5}N$ epilayers

After observing the presence of SAM, its effect on the roughness of $Al_{0.5}Ga_{0.5}N$ film was tested. AFM scans of both bare and SAM passivated films were recorded (figures 3(a) and (b)). The RMS value of roughness was found to reduce from 12.2 nm for bare film to 11.9 nm for the SAM passivated film, which implied a good quality surface passivation.

Since surface charge is represented by surface potential [35, 36], the KPFM scans of both the films were taken (figures 4(a) and (b)). The measured contact potential

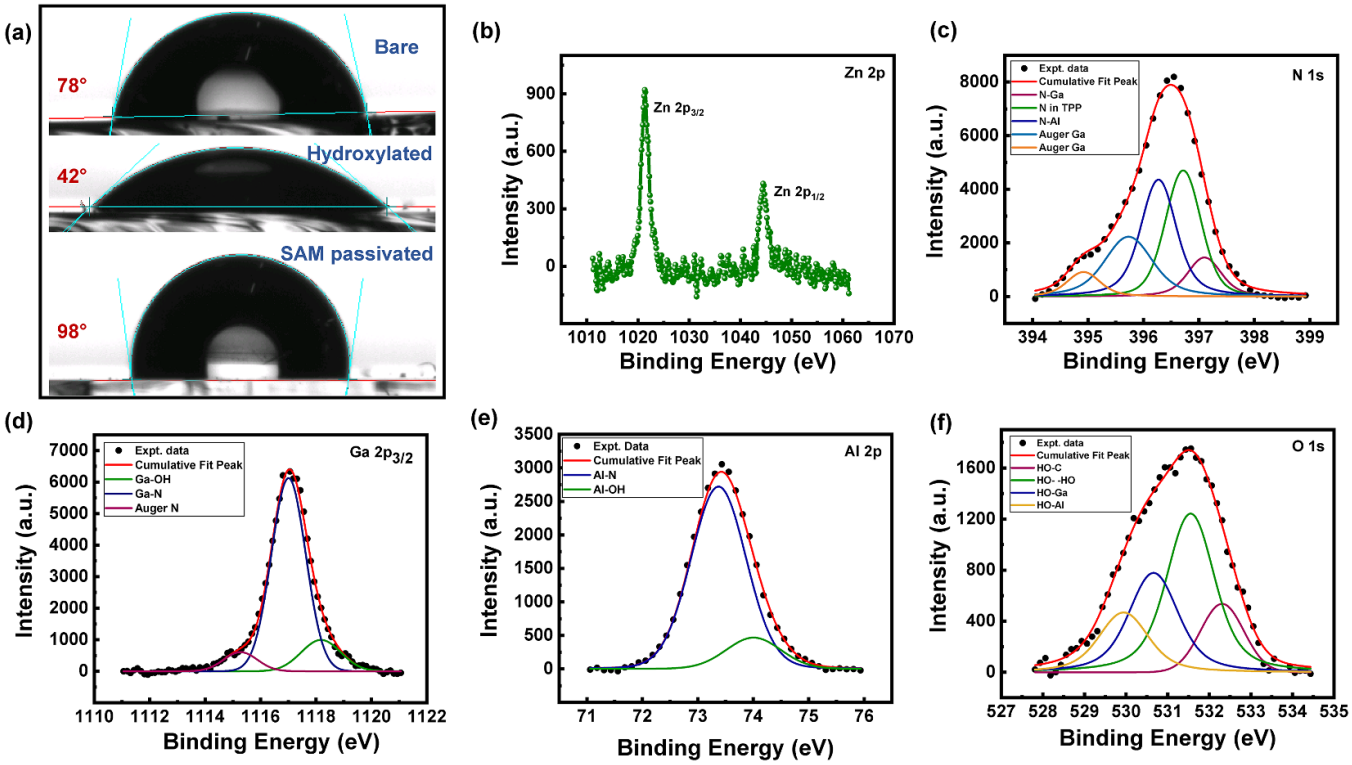

Figure 2. (a) The CAs for bare, hydroxylated, and SAM passivated $Al_{0.5}Ga_{0.5}N$ films. XPS peaks of (b) Zn 2p, (c) N 1s, (d) Ga $2p_{3/2}$, (e) Al 2p, and (f) O 1s for ZnTPP(OH) SAM passivated $Al_{0.5}Ga_{0.5}N$ films.

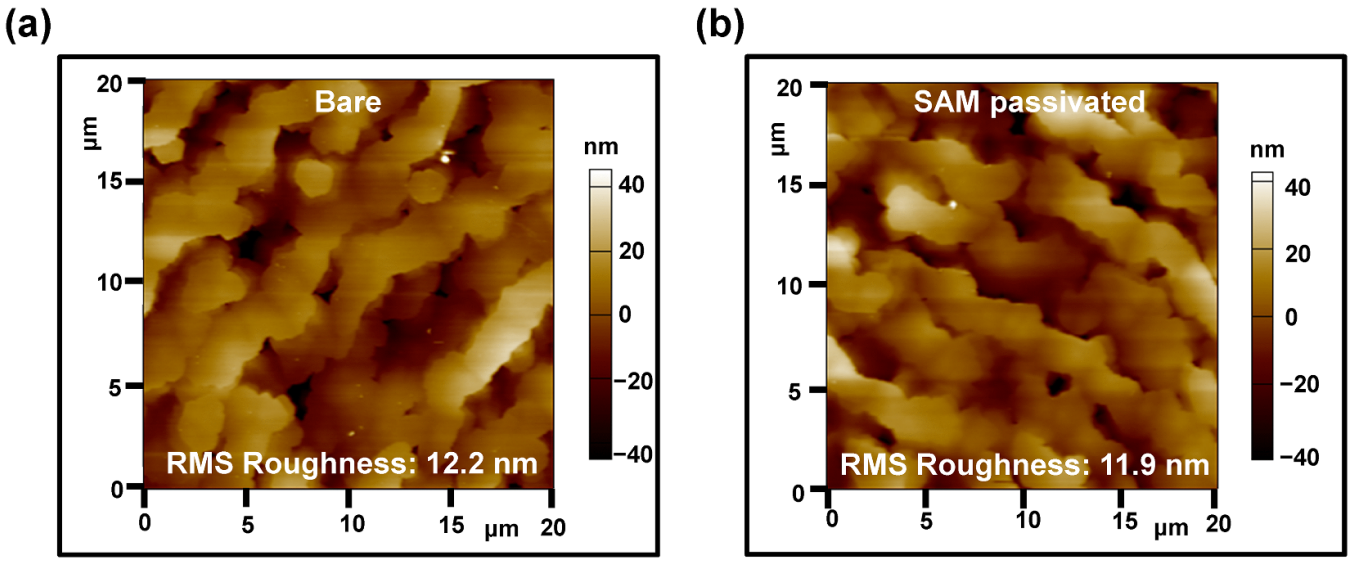

Figure 3. AFM images of (a) bare, and (b) SAM passivated $Al_{0.5}Ga_{0.5}N$ films.

difference by KPFM is related to the surface potential [36, 37]. Therefore, the measured potential values are directly related to the charges present on the film surface. As shown in figure 4(c), the mean value of surface potential for bare and passivated $Al_{0.5}Ga_{0.5}N$ films was found to be 560 and 282 mV, respectively. Since nitrogen vacancies and/or oxygen and silicon impurities lead to the unintentional *n*-type doping in III–V nitrides [38, 39], the presence of surface states leads to an upward band bending in AlGaN [18, 23]. The change in surface potential upon passivation reflects the change in band bending [37]. Therefore, a significant decrease in surface potential by 278 mV indicates a decrease in upward band bending, as shown in figures 4(d) and (e). This clearly highlights a decrease in surface charge and successful passivation of the surface states by SAM of porphyrin molecules.

The above results were also supported by PL spectroscopy. Figure 5 shows the PL spectra of bare and passivated $Al_{0.5}Ga_{0.5}N$ films, zoomed for near band-edge emission

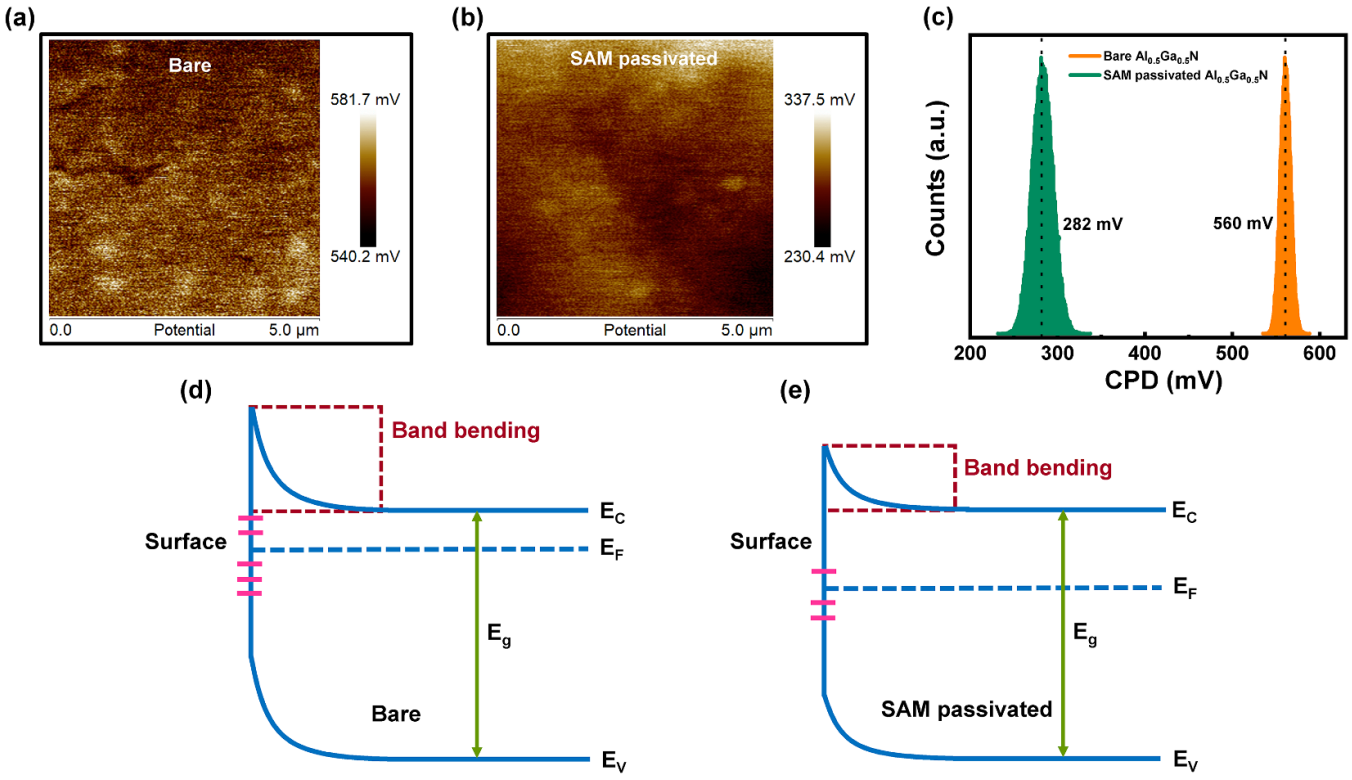

Figure 4. KPFM images of (a) bare, and (b) SAM passivated $Al_{0.5}Ga_{0.5}N$ films. (c) The plot showing the mean surface potential of bare and passivated films. The energy band diagrams highlighting (d) band bending in bare film, and (e) decrease in band bending in SAM passivated films.

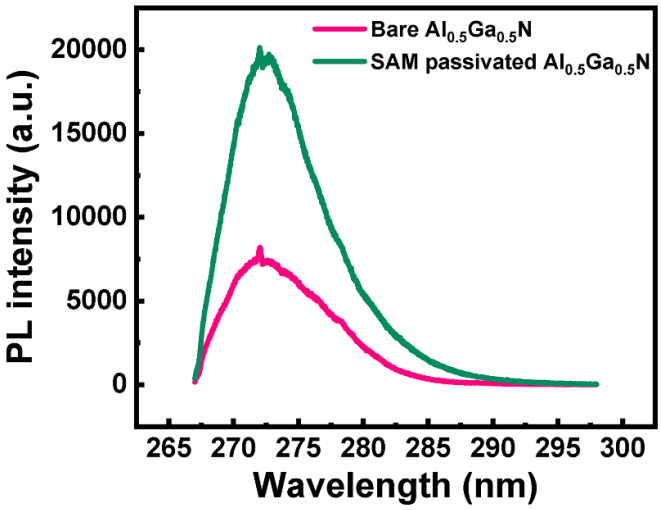

Figure 5. A comparison of PL intensity of NBE peak of the bare and SAM passivated $Al_{0.5}Ga_{0.5}N$ films.

(NBE) peak. As is clear from the figure, a four-fold increase in the PL intensity of NBE peak was observed for the SAM passivated film. An increase in the PL intensity reflects the higher probability of radiative recombination [40], and decrease in the surface recombination velocity [41]. Therefore, a significant enhancement in PL intensity of the NBE peak is attributed to the successful passivation of surface states by SAM.

3.3. Effect of SAM on $Al_{0.5}Ga_{0.5}N$ solar-blind photodetector

After examination of the effect of ZnTPP(OH) SAM on $Al_{0.5}Ga_{0.5}N$ epilayer, MSM photodetectors with 50 μm electrode width and inter-electrode spacing were fabricated on both bare and passivated samples and *I–V* and *I–t* measurements were performed. The semi-log plots of dark and photo currents versus voltage for Ni/Bare $Al_{0.5}Ga_{0.5}N$/Ni and Ni/SAM $Al_{0.5}Ga_{0.5}N$/Ni photodetectors are shown in figures 6(a) and (b), respectively. A comparison of the dark current of the two devices is shown in figure 6(c), which shows that the dark current of Ni/SAM $Al_{0.5}Ga_{0.5}N$/Ni photodetector was found to decrease by nearly two orders of magnitude (especially at high voltages), without degrading the magnitude of the photocurrent at 270 nm. For example, at −10 V, the dark current for photodetector fabricated on bare film was measured to be 4.8×10^{-8} A, while it was 5.4×10^{-10} A for the passivated film based photodetector. The effect of reduction of the dark current was manifested in the PDCR of the photodetector, which is given by [42–44]:

$$\mathrm{PDCR} = \frac{(I_{\mathrm{ph}} - I_{\mathrm{d}})}{I_{\mathrm{d}}} \tag{1}$$

where I_{ph} is the photo current at 270 nm and I_{d} is the dark current. As shown in figure 6(d), a significant enhancement in PDCR was observed for devices fabricated on the passivated films. The peak PDCR increased by ∼36 times (from 322 to 11 561).

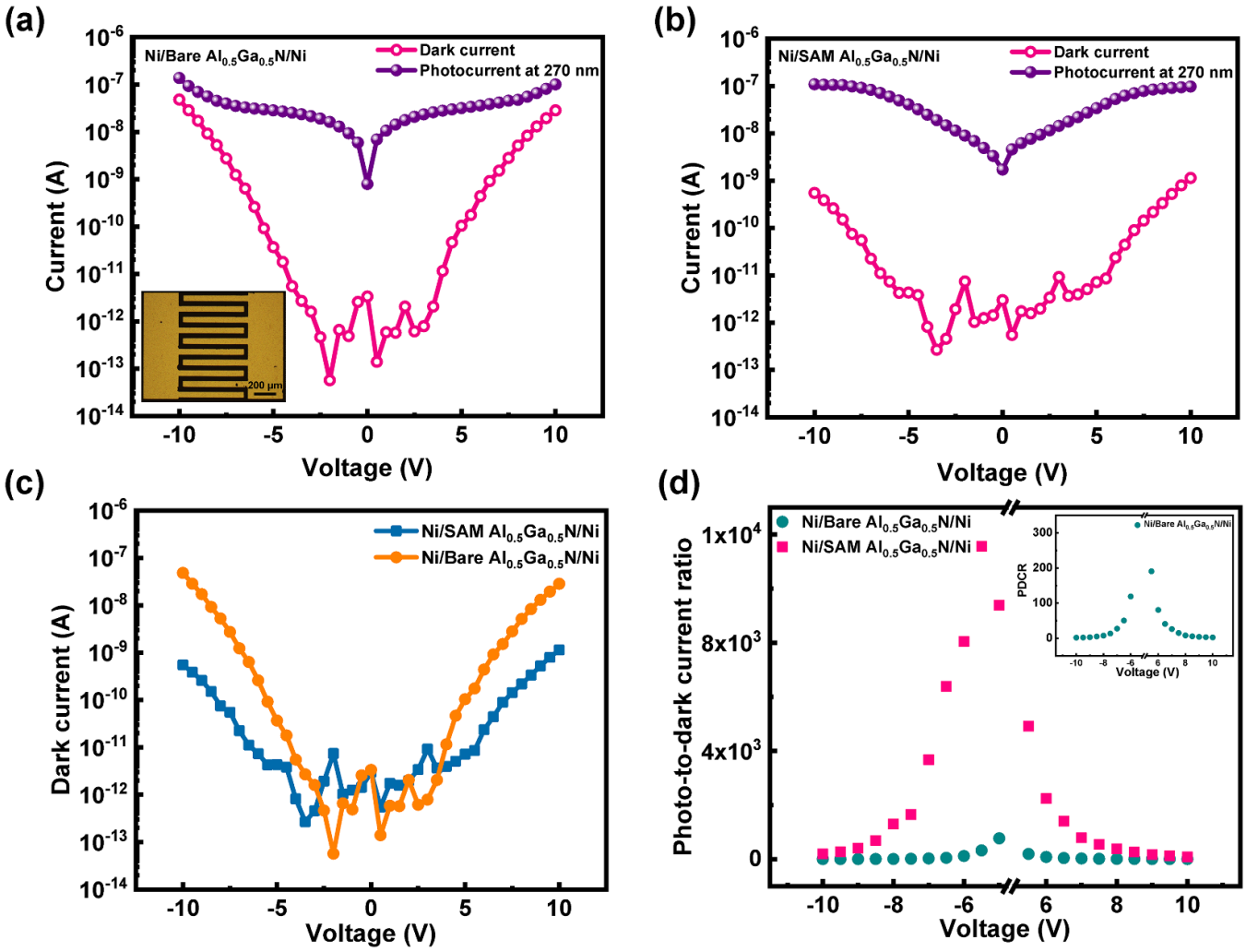

Figure 6. Dark and photo currents of (a) Ni/Bare $Al_{0.5}Ga_{0.5}N$/Ni, and (b) Ni/SAM $Al_{0.5}Ga_{0.5}N$/Ni photodetector. The inset in (a) shows the optical microscope image of as-fabricated MSM photodetector with interdigitated electrodes of width and spacing 50 μm each. A comparison of the (c) dark current, and (d) PDCR versus voltage of the two photodetectors. The inset in (d) shows zoomed PDCR of Ni/Bare $Al_{0.5}Ga_{0.5}N$/Ni photodetector.

Figure 7. shows the energy band diagram of MSM photodetectors fabricated on bare and SAM passivated $Al_{0.5}Ga_{0.5}N$ epitaxial films. Due to the presence of a large density of surface states in bare $Al_{0.5}Ga_{0.5}N$ film, the current transport mechanisms get modified. One of the prominent mechanisms is the TAT, which is shown in figure 7(a) [18–21]. As a result, a large dark current is observed for Ni/Bare $Al_{0.5}Ga_{0.5}N$/Ni photodetector. For Ni/SAM $Al_{0.5}Ga_{0.5}N$/Ni, a decrease in the dark current is attributed to the passivation of surface states of $Al_{0.5}Ga_{0.5}N$ by SAM. Due to passivation, the available tunneling pathways are no longer available to the carriers, leading to the less contribution of TAT to the dark current (as shown in figure 7(b)). Therefore, a significant decrease in dark current and enhancement in PDCR was observed for the photodetector fabricated on passivated $Al_{0.5}Ga_{0.5}N$ films.

Besides improving the PDCR, SAM also led to an improvement in the responsivity of the photodetector, which is expressed as [26, 43, 44]:

$$R_\lambda = \frac{(I_{ph} - I_d)}{P_\lambda} \tag{2}$$

where P_λ is the power of incident light of wavelength λ. Figure 8(a) shows the plot of responsivity of the two photodetectors versus wavelength. It is worth noting that the as-fabricated photodetectors were completely irresponsive up to 300 nm, and started giving a response only after 280 nm, thereby exhibiting the complete 'solar-blindness'. The maximum responsivity was observed at deep UV wavelength of 270 nm. The comparison shows that the responsivity increased from ∼0.9 mA W^{-1} to ∼1.6 mA W^{-1} at 7 V at the incident wavelength of 270 nm. On reducing the wavelength further, most of the light gets absorbed near the upper surface of the material instead of getting absorbed uniformly throughout the active region [45]. As a result, the responsivity of both the devices was found to decrease in the shortwave region. Moreover, the responsivity was found to increase with increase in the applied voltage, as shown in the inset of figure 8(a). A maximum value of 2.2 mA W^{-1} at 10 V was calculated for Ni/SAM $Al_{0.5}Ga_{0.5}N$/Ni photodetector by using the incident power density of only 2.62 μW mm^{-2}.

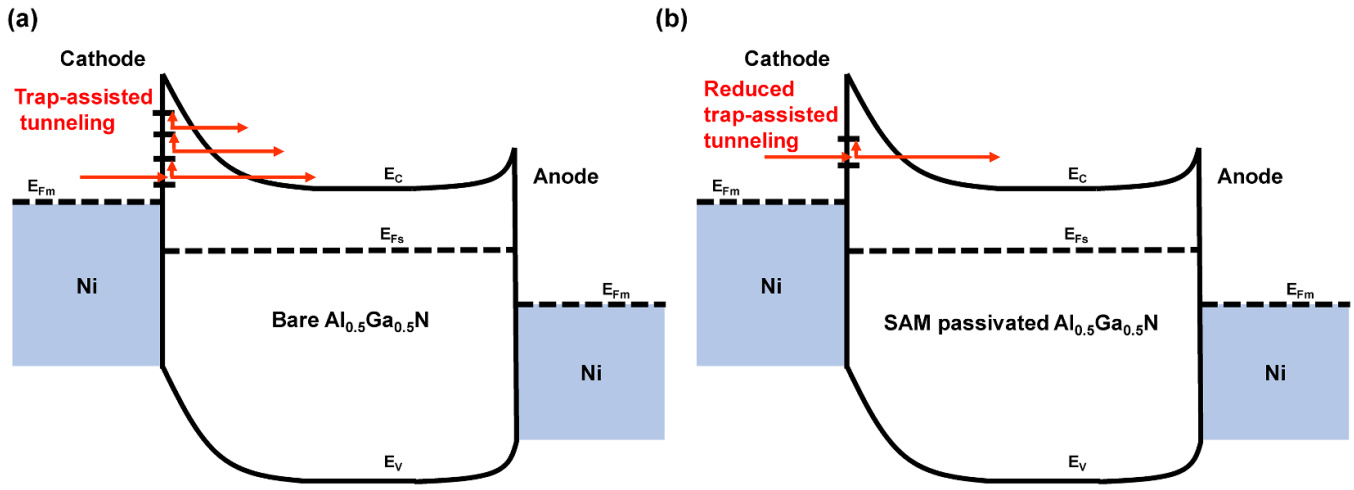

Figure 7. Energy band diagram of MSM photodetector fabricated on (a) bare, and (b) SAM passivated $Al_{0.5}Ga_{0.5}N$ epilayer.

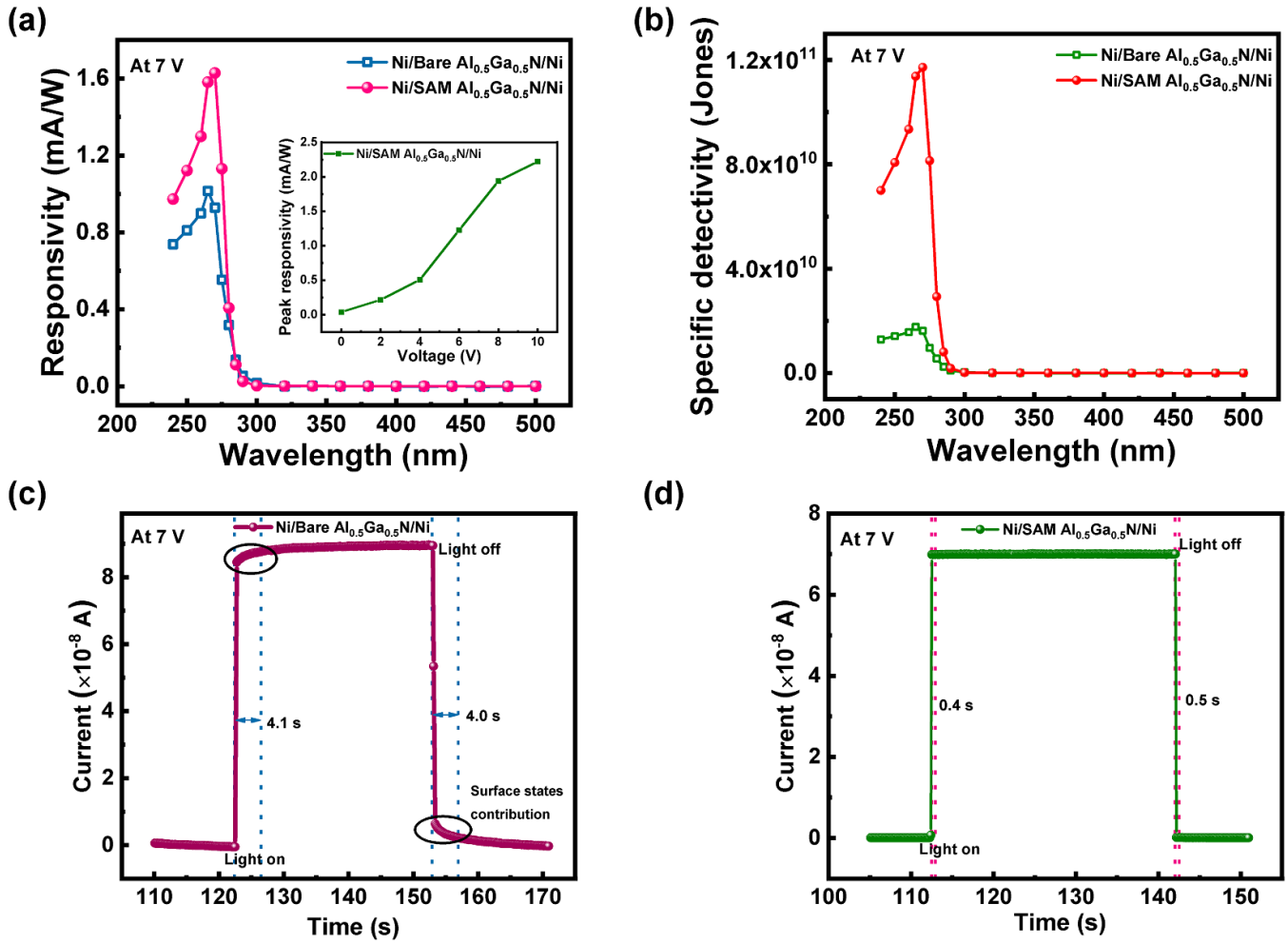

Figure 8. (a) The plot of responsivity versus incident wavelength of Ni/Bare $Al_{0.5}Ga_{0.5}N$/Ni and Ni/SAM $Al_{0.5}Ga_{0.5}N$/Ni photodetector. The inset shows the variation of peak responsivity with voltage for Ni/SAM $Al_{0.5}Ga_{0.5}N$/Ni photodetector. (b) The plot of specific detectivity versus incident wavelength for the two photodetectors. The temporal response of (c) Ni/Bare $Al_{0.5}Ga_{0.5}N$/Ni, and (d) Ni/SAM $Al_{0.5}Ga_{0.5}N$/Ni photodetector.

The sensitivity of a photodetector is measured in terms of the specific detectivity which is given by [46]

$$D^* = R_\lambda \sqrt{\frac{A}{2eI_d}} \tag{3}$$

where A is the area of device ($\sim$15 mm^2). Equation (3) implies that specific detectivity is related to the responsivity and dark current of the photodetector. The successful passivation of the surface states resulted in reduction in the dark current and enhancement in the responsivity. As a result, a significant improvement in the specific detectivity was observed for Ni/SAM $Al_{0.5}Ga_{0.5}N$/Ni photodetector. At 7 V, the specific detectivity was found to increase from 1.6×10^{10} to 1.2×10^{11} Jones for the photodetector fabricated on passivated $Al_{0.5}Ga_{0.5}N$ epilayer (figure 8(b)).

The successful passivation also resulted in improving the speed of the photodetector. The response of the Ni/Bare $Al_{0.5}Ga_{0.5}N$/Ni photodetector to the switching input signal (on/off) is shown in figure 8(c). On switching the light on (or off), a sudden change in carrier concentration results in sharp rise (or fall) of the current. Along with these fast components, slow rising (or falling) edges can also be seen. These reflect the degrading effect of surface states on the speed of the photodetector. The surface states act as traps for the carriers and slow down the response speed of the device [27, 47]. For Ni/Bare $Al_{0.5}Ga_{0.5}N$/Ni photodetector, an approximate rise and fall time of 4 s was observed. On comparing the response to Ni/SAM $Al_{0.5}Ga_{0.5}N$/Ni photodetector, a clear reduction in the response time to $\sim$0.5 s was noted (figure 8(d)). This improvement in the speed of the photodetector is attributed to the effective passivation of surface states of $Al_{0.5}Ga_{0.5}N$ by SAM, which suppressed the slow components of rise (or fall) time.

The results show that the SAM led to a significant improvement in the performance of the $Al_{0.5}Ga_{0.5}N$-based solar-blind MSM photodetector. The enhancement in PDCR, responsivity and specific detectivity is attributed to a reduction in the dark current by successful passivation of the surface states of $Al_{0.5}Ga_{0.5}N$ by SAM. Moreover, ZnTPP(OH) is stable up to 460 °C [28]; therefore, the fabricated photodetector is expected to exhibit high temperature robustness. However, the radiation and chemical hardness of the photodetector will be limited by the SAM and needs to be explored further.

4. Conclusions

In conclusion, the surface states of $Al_{0.5}Ga_{0.5}N$ were successfully passivated by SAM of ZnTPP(OH) molecules, which led to a drastic improvement in the performance of the fabricated solar-blind photodetector. The molecular layer was characterized by CA, XPS and AFM. A clear reduction in the surface potential by $\sim$280 mV and a four-fold increase in the PL intensity confirmed the passivation of surface states. As a result, a significant reduction in the dark current by two orders of magnitude, enhancement in peak PDCR by $\sim$36 times and specific detectivity by $\sim$10 times, improvement in peak responsivity from 1.6 to 2.2 mA W^{-1}, and in temporal response from 4 s to 0.5 s was observed for the SAM passivated $Al_{0.5}Ga_{0.5}N$ based solar-blind photodetector.

Data availability statement

All data that support the findings of this study are included within the article (and any supplementary files).

Acknowledgments

S K acknowledges Ministry of Education, Govt. of India for providing the fellowship. The authors are grateful to IITBNF for CA, AFM and XPS characterizations; SSPL, DRDO for PL and IITD NRF for KPFM, device fabrication and characterization facilities.

Conflict of interest

The authors declare no competing interests.

ORCID iDs

Shuchi Kaushik https://orcid.org/0000-0002-1927-7945
Xiaohang Li https://orcid.org/0000-0002-4434-365X
R Singh https://orcid.org/0000-0002-6890-6904

References

[1] Zheng W, Jia L and Huang F 2020 Vacuum-ultraviolet photon detections *iScience* **23** 101145
[2] Zheng W, Lin R, Ran J, Zhang Z, Ji X and Huang F 2018 Vacuum-ultraviolet photovoltaic detector *ACS Nano* **12** 425–31
[3] Li Y, Zheng W and Huang F 2020 All-silicon photovoltaic detectors with deep ultraviolet selectivity *PhotoniX* **1** 15
[4] Vatansever F, Ferraresi C, De Sousa M V P, Yin R, Rineh A, Sharma S K and Hamblin M R 2013 Can biowarfare agents be defeated with light? *Virulence* **4** 37–41
[5] Razeghi M and Rogalski A 1996 Semiconductor ultraviolet detectors *J. Appl. Phys.* **79** 7433–73
[6] Welch D, Buonanno M, Grilj V, Shuryak I, Crickmore C, Bigelow A W, Randers-Pehrson G, Johnson G W and Brenner D J 2018 Far-UVC light: a new tool to control the spread of airborne-mediated microbial diseases *Sci. Rep.* **8** 2752
[7] Ulmer M P, Razeghi M, Bigan E and Science C 1995 Ultra-violet detectors for astrophysics, present and future *Optoelectron. Integr. Circuit Mater. Phys. Devices* **2397** 210–7
[8] Razeghi M 2002 Short-wavelength solar-blind detectors—status, prospects, and markets *Proc. IEEE* **90** 1006–14
[9] BenMoussa A *et al* 2009 Recent developments of wide-bandgap semiconductor based UV sensors *Diam. Relat. Mater.* **18** 860–4
[10] Arora K, Singh D P, Fischer P and Kumar M 2020 Spectrally selective and highly sensitive UV photodetection with UV-A,C band specific polarity switching in silver plasmonic nanoparticle enhanced gallium oxide thin-film *Adv. Opt. Mater.* **8** 2000212

[11] Angerer H *et al* 1997 Determination of the Al mole fraction and the band gap bowing of epitaxial AlxGa1-XN films *Appl. Phys. Lett.* **71** 1504–6

[12] Monroy E, Calle F, Muñoz E and Omnès F 1999 AlGaN metal-semiconductor-metal photodiodes *Appl. Phys. Lett.* **74** 3401–3

[13] Averine S V, Kuznetzov P I, Zhitov V A and Alkeev N V 2008 Solar-blind MSM-photodetectors based on AlxGa1-XN/GaN heterostructures grown by MOCVD *Solid State Electron.* **52** 618–24

[14] Li J, Zhao M and Wang X F 2010 High performance Schottky UV photodetectors based on epitaxial AlGaN thin film *Physica* B **405** 996–8

[15] Xie F, Lu H, Chen D, Ji X, Yan F, Zhang R, Zheng Y, Li L and Zhou J 2012 Ultra-low dark current AlGaN-based solar-blind metal-semiconductor-metal photodetectors for high-temperature applications *IEEE Sens. J.* **12** 2086–90

[16] Li D, Jiang K, Sun X and Guo C 2018 AlGaN photonics: recent advances in materials and ultraviolet devices *Adv. Opt. Photonics* **10** 43

[17] Strite S, Lin M E and Morkoç H 1993 Progress and prospects for GaN and the III–V nitride semiconductors *Thin Solid Films* **231** 197–210

[18] Eller B S, Yang J and Nemanich R J 2013 Electronic surface and dielectric interface states on gan and algan *J. Vac. Sci. Technol.* A **31** 50807

[19] Carrano J C, Li T, Grudowski P A, Eiting C J, Dupuis R D and Campbell J C 2004 Current transport mechanisms in GaN-based metal–semiconductor–metal photodetectors *Appl. Phys. Lett.* **542** 542–4

[20] Miller E J, Yu E T, Waltereit P and Speck J S 2004 Analysis of reverse-bias leakage current mechanisms in GaN grown by molecular-beam epitaxy *Appl. Phys. Lett.* **84** 535–7

[21] Karmalkar S, Sathaiya D M and Shur M S 2003 Mechanism of the reverse gate leakage in AlGaN/GaN high electron mobility transistors *Appl. Phys. Lett.* **82** 3976–8

[22] Sun H, Shakfa M K, Muhammed M M, Janjua B, Li K H, Lin R, Ng T K, Roqan I S, Ooi B S and Li X 2018 Surface-passivated AlGaN nanowires for enhanced luminescence of ultraviolet light emitting diodes *ACS Photonics* **5** 964–70

[23] Zhang Z and Yates J T 2012 Band bending in semiconductors: chemical and physical consequences at surfaces and interfaces *Chem. Rev.* **112** 5520–51

[24] Schreiber F 2000 Structure and growth of self-assembling monolayers *Prog. Surf. Sci.* **65** 151–257

[25] Ulman A 1996 Formation and structure of self-assembled monolayers *Chem. Rev.* **96** 1533–54

[26] Kaushik S, Naik T R, Alka A, Garg M, Tak B R, Ravikanth M, Rao V R and Singh R 2020 Surface modification of AlN using organic molecular layer for improved deep UV photodetector performance *ACS Appl. Electron. Mater.* **2** 739–46

[27] Garg M, Tak B R, Rao V R and Singh R 2019 Giant UV photoresponse of GaN-based photodetectors by surface modification using phenol-functionalized porphyrin organic molecules *ACS Appl. Mater. Interfaces* **11** 12017–26

[28] Naik T R, Singh V, Ravikanth M and Rao V R 2016 A vapor phase self-assembly of porphyrin monolayer as a copper diffusion barrier for back-end-of-line CMOS technologies *IEEE Trans. Electron Devices* **63** 2009–15

[29] Baur B, Steinhoff G, Hernando J, Purrucker O, Tanaka M, Nickel B, Stutzmann M and Eickhoff M 2005 Chemical functionalization of GaN and AlN surfaces *Appl. Phys. Lett.* **87** 263901

[30] Garg M, Naik T R, Pathak R, Rao V R, Liao C H, Li K H, Sun H, Li X and Singh R 2018 Effect of surface passivation process for AlGaN/GaN HEMT heterostructures using phenol functionalized-porphyrin based organic molecules *J. Appl. Phys.* **124** 195702

[31] Garg M, Naik T R, Pathak C S, Nagarajan S, Rao V R and Singh R 2018 Significant improvement in the electrical characteristics of Schottky barrier diodes on molecularly modified gallium nitride surfaces *Appl. Phys. Lett.* **112** 163502

[32] Lavallee D K, Brace J and Winograd N 1979 X-ray photoelectron spectra of JV-methyltetraphenylporphyrins: evidence for a correlation of binding energies with metal-nitrogen bond distances *Inorg. Chem.* **18** 1776–80

[33] Rosenberger L, Baird R, McCullen E, Auner G and Shreve G 2008 XPS analysis of aluminum nitride films deposited by plasma source molecular beam epitaxy *Surf. Interface Anal.* **40** 1254–61

[34] Kerber S J, Bruckner J J, Wozniak K, Seal S, Hardcastle S and Barr T L 2002 The nature of hydrogen in x-ray photoelectron spectroscopy: general patterns from hydroxides to hydrogen bonding *J. Vac. Sci. Technol.* A **14** 1314–20

[35] Lee H, Lee W, Lee J H and Yoon D S 2016 Surface potential analysis of nanoscale biomaterials and devices using kelvin probe force microscopy *J. Nanomater.* **2016** 1–21

[36] Kwon O and Kim Y 2014 Probing of surface potential using atomic force microscopy *Appl. Microsc.* **44** 100–4

[37] Melitz W, Shen J, Kummel A C and Lee S 2011 Kelvin probe force microscopy and its application *Surf. Sci. Rep.* **66** 1–27

[38] Van De Walle C G, Stampfl C and Neugebauer J 1998 Theory of doping and defects in III–V nitrides *J. Cryst. Growth* **189–190** 505–10

[39] Sheu J K and Chi G C 2002 The doping process and dopant characteristics of GaN *J. Phys.: Condens. Matter* **14** R657–702

[40] Zhao C *et al* 2015 An enhanced surface passivation effect in InGaN/GaN disk-in-nanowire light emitting diodes for mitigating Shockley–Read–Hall recombination *Nanoscale* **7** 16658–65

[41] Kumar A, Singh T, Kumar M and Singh R 2014 Sulphide passivation of GaN based Schottky diodes *Curr. Appl. Phys.* **14** 491–5

[42] Qiao H, Huang Z, Ren X, Liu S, Zhang Y, Qi X and Zhang H 2020 Self-powered photodetectors based on 2D materials *Adv. Opt. Mater.* **8** 1900765

[43] Sorifi S, Moun M, Kaushik S and Singh R 2020 High-temperature performance of a GaSe nanosheet-based broadband photodetector *ACS Appl. Electron. Mater.* **2** 670–6

[44] Kaushik S, Sorifi S and Singh R 2021 Study of temperature dependent behavior of H-BN nanoflakes based deep UV photodetector *Photon. Nanostruct: Fundam. Appl.* **43** 100887

[45] Burger P R 1996 Metal-semiconductor-metal photodetectors *IEEE Potentials* **15** 25–28

[46] Wang F *et al* 2018 2D library beyond graphene and transition metal dichalcogenides: a focus on photodetection *Chem. Soc. Rev.* **47** 6296–341

[47] Guo X C, Hao N H, Guo D Y, Wu Z P, An Y H, Chu X L, Li L H, Li P G, Lei M and Tang W H 2016 β-Ga2O3/p-Si heterojunction solar-blind ultraviolet photodetector with enhanced photoelectric responsivity *J. Alloys Compd.* **660** 136–40